

Direct Preparation of Carbon Nanofiber Electrodes via Pyrolysis of Iron(II) Phthalocyanine: Electrocatalytic Aspects for Oxygen Reduction

Stephen Maldonado and Keith J. Stevenson*

Department of Chemistry and Biochemistry, Center for Nano- and Molecular Science and Technology, Texas Materials Institute, The University of Texas at Austin, Austin, Texas 78712

Received: January 23, 2004; In Final Form: May 27, 2004

A facile method for the direct preparation of carbon nanofiber (CNF) electrodes by pyrolysis of iron(II) phthalocyanine on nickel substrates is reported. Uniform, large area coverage is observed with aligned bundles of CNFs exhibiting bamboo-like, hollow fibril morphology possessing diameters of 40–60 nm and lengths of $\sim 10 \mu\text{m}$. The electrochemical behavior and stability of CNF electrodes as oxygen reduction catalysts were investigated by electrochemical methods. Without necessitation for extensive electrode pretreatment or surface activation, these electrodes demonstrate significant electrocatalytic activity in aqueous KNO_3 solutions at neutral to basic pH for the reduction of dioxygen to hydrogen peroxide, $\text{O}_2 + \text{H}_2\text{O} + 2\text{e}^- \rightleftharpoons \text{HO}_2^- + \text{OH}^-$. As determined from chronocoulometry, slopes of Anson plots indicate that the overall electrochemical reaction proceeds by the peroxide pathway via two successive two-electron reductions. pH-dependent cyclic voltammetry studies indicate that the CNF electrodes are very active toward adsorption. At $\text{pH} < 10$ the one-electron reduction of O_2 to superoxide is rate limiting, whereas at more alkaline pH the reduction process is limited by the protonation of adsorbed superoxide. This is reflected by a change in measured apparent charge-transfer coefficient (α_{obs}) from $\alpha_{\text{obs}} = 0.5$ to $\alpha_{\text{obs}} = 1$ at neutral and high pH values, respectively. XPS, Raman, and TEM measurements suggest that the disorder in the graphite fibers and the presence of exposed edge plane defects and nitrogen functionalities are important factors for influencing adsorption of reactive intermediates and enhancing electrocatalysis for O_2 reduction.

Introduction

Carbon materials possess suitable properties for the design of electrodes used in electrochemical devices because of their relative stability, conductivity, high surface area, and chemical resistance. Although the literature for carbon-based electrodes is rich in studies with traditional forms of carbon¹ (i.e., carbon blacks, pyrolytic graphite, and glassy carbon), much less attention has been given to nanotubular structured electrode materials, i.e., hollow carbon nanofibers (CNFs), single-wall carbon nanotubes (SWCNTs), and multiwall carbon nanotubes (MWCNTs). Historically, the usage of the “nanofiber” nomenclature predates the “nanotube” vernacular by more than a century and inherently associates key properties of nanoscale fibers and filamentous carbons that are often understressed, e.g., the presence of metal catalysts, the turbostratic graphitic nature, and the amount of basal/edge plane graphite.^{2–4} Importantly, we point out that usage of “CNT” and “MWCNT” terminology and various other acronyms in recent literature, however, is inconsistent and vague, given that several forms of nanotubular carbon (e.g., straight, corkscrew, fishbone, platelet, and bamboo) have been prepared with both extremely narrow diameters (~ 2 nm) and much larger diameters (~ 200 nm). As recently emphasized by Sinnott and Andrews,⁴ nanotubes and nanofibers are similar materials that are differentiated predominantly by the characteristic alignment of graphite crystallites within their wall structure, with the least ordered of these materials being carbon nanofibers. Since inherent carbon electrode properties have a profound effect on observed electrochemical behavior

such as capacitance, electron-transfer rates, and adsorption, it is important to distinguish accurately the particular type of carbon under study and to describe carefully not only structural features but also the chemical properties as well. Correlation of carbon electrode characteristics with electrochemical performance is extremely difficult and definite connections between structure, composition, and electroactivity can only be established when well-defined systems such those detailed by McCreery⁵ are systematically studied. We emphasize these points not merely for semantics, but also (1) to historically recognize and stay consistent with the many decades of research in the area of carbon nanofibers,^{3,6} and (2) to distinguish between the thin, idealized CNTs (diameters $\ll 30$ nm) of structural perfection that have been the focus of quantum theory-driven spectroscopic studies⁷ from larger diameter (> 30 nm), more disordered CNFs that have been the focus of most of the practical device applications (e.g., batteries, fuel cells, displays).^{1,5,8,9} Since quantum effects are not observed in nanotubes larger than ~ 30 nm, many investigators have proposed that these materials be more generally referred to as carbon nanofibers (CNFs) and not CNTs or MWCNTs.¹⁰ Respectfully, we too have adopted this convention and refer to the materials described herein as CNFs.

A particularly attractive approach for synthesizing high surface area carbon electrodes is one that is based on chemical vapor deposition (CVD) using metallocenes^{11,12} or metallophthalocyanines^{13,14} that function simultaneously as both the growth catalyst and carbon source.¹⁵ This method offers the most promise for high-throughput, large-scale preparation of vertically aligned, high-density, multiwalled carbon nanofibers. While

* Author to whom correspondence should be addressed. E-mail: stevenson@mail.cm.utexas.edu.

some have reported success in the direct growth of CNTs and CNFs on conductive substrates^{16–21} using a variety of methodologies, very few careful studies have been performed fully to evaluate innate electrochemical properties. Most reports describe the characterization of SWCNT, MWCNT, and CNF electrodes prepared by filtering a suspension of these materials and casting onto a conductive support.^{22–24} Others have relied upon lift-off of the carbon film from its growth substrate, typically an insulator such as silicon or quartz, and gross transfer onto a conductive surface, e.g., gold, and attachment via compaction,^{25,26} conductive epoxy,^{27–29} and/or binding agents.^{30–35} In the former case, the redispersed carbon films typically comprise poorly adherent, uneven mats of dense, randomly entangled CNFs or CNTs. This arrangement suffers from mechanical instability, obstructed surface area, and porosity, and effectively imposes kinetic and mass transport constraints on the electrochemical system. In the latter case, reattachment of carbon materials to conductive supports using foreign conductive agents is nontrivial and the effects of material processing, physical transfer, and added chemical components are poorly understood and/or recognized.

Herein, we report the facile preparation of vertically aligned CNF electrodes produced directly on conductive supports without the necessity of excessive pre- or post-treatment or chemical surface activation. An attractive feature of these CNF electrodes is that the fabrication is inherently easier, quicker, and more controllable than traditional methods for making high surface area carbon electrodes. This route also allows for simultaneous doping of heteroatoms and other species into fibril structure during the growth process to prepare chemically modified CNFs. Additionally, the inherent carbon properties (i.e., orientation, alignment, crystallinity, composition) can be systematically tuned by precise adjustment of the growth conditions. This approach also facilitates the careful study of inherent electrochemical properties of “as grown” CNF electrodes. Preliminary studies of CNF electrodes prepared using an iron(II) phthalocyanine precursor demonstrate high electrocatalytic ability for the reduction of dissolved dioxygen at neutral to basic pH values. The influence of structural and compositional properties on manifested electron transfer and dioxygen electrocatalysis behaviors is discussed.

Experimental Section

CNF Electrode Preparation. Nickel mesh (Alfa Aesar, 100 mesh) was cut into 0.40 cm² squares prior to CNF growth using a razor blade. Using a modified method of that described by Huang et al.,¹⁴ the pyrolysis of iron(II) phthalocyanine (Aldrich, used as received and hereafter denoted as FePc) on nickel mesh substrates was performed at 1000 °C in a reducing atmosphere of Ar–H₂ (99.997 and 99.95%, respectively, Praxair) in a gas flow reactor consisting of a quartz tube (35 mm OD, 32 mm ID) and a two-zone tube furnace (Thermcraft, model 2158-6-3ZH) fitted with temperature controllers. Prior to growth, nickel mesh substrates were inserted into zone 2 of the furnace and the quartz tube was purged with Ar for ~10 min. Subsequently, a mixture of Ar and H₂ gases (0.8:1 ratio) was introduced to the furnace at 45 cm³/min (cubic centimeter per minute) while the two zones were heated to defined temperatures (zone 1 at 500 °C, and zone 2 at 1000 °C). When the cooler (upstream) zone 1 reached 500 °C, 0.2 g of FePc was introduced and nanofiber growth was allowed to occur for 5 min. The temperature of zone 1 was then ramped up to 1000 °C and held at this temperature for an additional 15 min. The furnace was then turned off and the carbon nanofiber (CNF) electrodes were

allowed to cool in the furnace. When the system had cooled to 850 °C, the H₂ flow was stopped while, simultaneously, the Ar flow was increased to 45 cm³/min to maintain a constant total gas flow. Once the furnace had cooled to room temperature, the CNF electrodes were removed from the quartz tube and stored in sealed gas-tight vials prior to structural and electrochemical characterization. The resulting CNF films appeared on the nickel mesh substrate as a fine, uniform black felt-like or carpet-like layer. The nominal mass of CNF coating the nickel mesh prepared in this manner was ~1 mg for all electrodes studied. All CNF electrodes used in this study were reproducibly prepared and possessed very similar structural and chemical characteristics.

Structural Characterization. Scanning electron microscopy (SEM) of the resultant CNF electrodes was carried out on a LEO 1530 operating at 10 kV. Transmission electron microscopy (TEM) was performed on a JEOL 2010F operating at 200 kV. TEM samples were prepared by first suspending collected CNFs in ethanol and then placing a drop of the suspension on a copper grid (200 mesh, PELCO) with a thin carbon coating. Surface analysis of the CNFs was performed by X-ray photoelectron spectroscopy (XPS) using a PHI 5700 ESCA system equipped with Al K α monochromatic (1486.6 eV) photons. Photoelectron spectra were recorded for the C1s, N1s, O1s, Fe2p_{1/2}, and Fe2p_{3/2} core levels. The low iron surface concentration required 10 scans averaged together to resolve the Fe 2p spectrum. All spectra are referenced to low, medium, and high photoelectron energy ranges using Au4f_{7/2}, Ag3d_{5/2}, and Cu2p_{3/2} at 83.98, 36.27, and 932.67 eV, respectively. Raman analysis was performed with a Renishaw InVia system using 514 nm incident radiation. A 50 \times aperture was used, resulting in approximately a 2 μ m spot size. TGA analysis was performed using a TA Instruments Q500 system.

Electrochemical Characterization. A single glass compartment, three-electrode, gas-tight electrochemical cell was employed for the cyclic voltammetry and chronocoulometry studies. Pt mesh (Aldrich) and Hg/Hg₂SO₄ (saturated K₂SO₄, CH Instruments) were used as the counter and reference electrodes, respectively, while CNF/nickel mesh or glassy carbon (GC) served as the working electrode. The GC electrode (Pine Instruments, model AFE2M050GC) was used after polishing with 0.3 and 0.05 μ m diameter alumina slurries. All electrode potentials are reported versus Hg/Hg₂SO₄ (saturated K₂SO₄), which is ca. 0.64 V positive of NHE. All electrochemical measurements were taken with a quiescent solution. The electrochemical cell temperature was held at a constant temperature (23.0 \pm 0.5 °C) by placement in a water bath. The electrochemical studies were performed with either a CH Instruments 700A potentiostat or an Autolab PGSTAT 30 interfaced to a PC.

Geometric surface areas of the CNF electrodes were determined by chronocoulometry (CC) using hexaammineruthenium(III) chloride (Strem Chemicals) in 1 M KNO₃. The potentials of the uncoated nickel mesh electrodes were stepped from –0.4 V to –0.8 V vs Hg/Hg₂SO₄ (saturated K₂SO₄) for 1 s and the area was calculated from the slope ($m = 2nFAD_o^{1/2}C\tau^{-1/2}$) of the linear portion of the Q vs $t^{1/2}$ plot (Anson plot) using the diffusion coefficient, $D_o = 7.3 \times 10^{-6}$ cm² s, determined by the steady-state current ($i_{lim} = 4nFD_oCr$) of a platinum microelectrode with $r = 13$ μ m. For uncoated nickel mesh electrodes, the observed electroactive area was 1.1 \pm 0.1 cm². Because the diffusion layer thickness for all measurements was sufficiently large ($(Dt)^{1/2} = 16$ μ m for the shortest experimental time, $\nu = 100$ mV/s), the diffusion layer was assumed to follow

the overall exposed nanofiber area rather than individual porous nanotubular morphology. The geometric surface areas of the CNF electrodes were assumed to be the same equivalent area as the uncoated nickel mesh electrodes.

For cyclic voltammetry and chronoamperometry studies, Ar or O₂ (99.5%, Praxair), introduced through a gas inlet of the electrochemical cell, was bubbled through the test solutions for 20 min prior to the start of the measurements (to either fully purge or to fully oxygenate, respectively) and again for one minute between measurements. Solution volumes were ~5–10 mL. The cell was kept at ambient pressure. O₂ partial pressures were measured using a mercury manometer connected to the cell. Dissolved O₂ concentrations were calculated using the Bunsen coefficient (i.e., Henry's Law constant) for oxygen solubility in 1 M KNO₃ at 25 °C.³⁶ The diffusivity of dissolved O₂, assumed to be $1.75 \times 10^{-5} \text{ cm s}^{-1}$,³⁷ was used in calculations involving chronocoulometry (Anson slopes). The solution was stirred while the cell was being pressurized and also prior to and after each electrochemical experiment. Electrolyte solutions were prepared using potassium nitrate (EM Science, 99.9%), sodium hydroxide (Aldrich, 99.99%), and/or boric acid (Spectrum, 99.9%) as received. The solutions with pH values 5.1 to 10.6 had formal concentrations of 0.9 M KNO₃ and 0.1 M H₃BO₃. The pH was adjusted by adding small aliquots of concentrated NaOH. The solution with a pH of 12.6 was made with 1 M KNO₃ and a small amount of NaOH added. The solution with a pH of 14 was 1 M NaOH. Cyclic voltammograms in the presence of O₂ were obtained by sweeping the potential from -0.2 V to -0.9 V at various sweep rates between 5 mV/s and 100 mV/s in corresponding supporting electrolytes. All CVs conducted in the presence of O₂ are background subtracted. Chronoamperometry studies for O₂ reduction were performed using a single potential-step method, stepping from an initial potential of -0.3 V to a final potential of -0.7 V potential and recording the charge passed for a period of one second.

Results and Discussion

CNF Electrode Structure and Composition. Figure 1 shows representative scanning electron microscopy (SEM) images of "as grown" CNF electrodes where a homogeneous distribution of CNFs on the nickel mesh support is seen and no discernible uncoated spots or bare regions are observed. Figure 1D demonstrates that the film maintains its conformal shape even after the removal of the underlying substrate. As detailed recently,³⁸ aligned growth of CNFs from FePc is believed to occur via a base-catalyzed, diffusion-controlled mechanism where iron nanoparticles serve as nucleation sites with CNFs growing upward as phthalocyanine molecules dissociate and dissolve on the molten catalytic surface. The produced material consists of carpet- or felt-like structures of carbon fibers that are fairly uniform (Figure 1B) and aligned normal to the nickel mesh support (Figure 1C), with lengths greater than 10 μm and diameters ranging from 40 to 60 nm. Transmission electron microscopy (TEM) images, Figure 2, show the hollow interior and disordered exterior structure of individual nanofibers. The presence of metallic Fe nanoparticles within the CNF interior is sometimes observed in the TEM imaging experiments. TEM coupled with PEELS analysis shows that the Fe nanoparticles still present within the CNFs are predominantly encapsulated within graphitic envelopes. We see no evidence for the existence of bare Fe particles on the exterior CNF surface. Higher magnification TEM images displayed in Figure 2B, reveal more details of the hollow fibril structure comprising irregular and

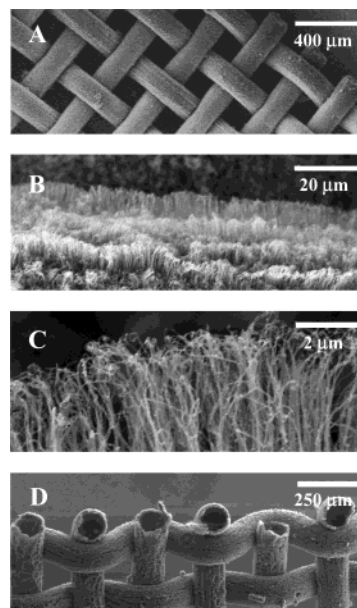


Figure 1. SEM images of a CNF electrode prepared by pyrolysis of FePc. (A) A low-resolution, large-area micrograph showing nickel mesh support structure. (B) A higher-resolution micrograph showing local micro-/nano-structure of CNFs. (C) A perpendicular view of the CNF electrode showing nanofiber alignment. (D) A micrograph of a free-standing, interwoven carbon mesh comprising bundles of CNFs produced by the removal of the growth substrate.

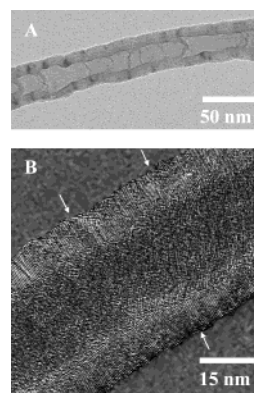


Figure 2. TEM images of typical CNFs prepared by pyrolysis of FePc showing compartmentalized, hollow fibril structure. (A) A low-resolution view of a nanofiber displaying numerous kinks and dislocations along its length. (B) A high-resolution micrograph illustrating breaks in the graphene layers where edge plane graphite defects are exposed (highlighted by white arrows).

interlinked corrugated features, consistent with other reports describing the preparation of N-doped nanotubes.^{38,39} Straight segments of parallel aligned graphene sheets of the CNFs appear crystalline and ordered over 10's of nm distances with the more crystalline domains intersecting disordered regions to produce compartmentalized, bamboo-like structures. The substitution of N atoms into the graphene structure favors the formation of pentagonal-like defects and is most likely responsible for the compartmentalized-like morphology. Presumably, these defects introduce dislocations and curvature into the nanofiber and correspond to sites where N-doped edge plane graphitic carbon and nitrogen-containing functional groups are exposed at the sidewalls.³⁸ A few of these regions are highlighted by white arrows in Figure 2B.

First-order Raman spectra were acquired to assess the relative amount of basal and edge plane graphite.⁴⁰ A representative Raman spectrum indicative of the existence of edge plane

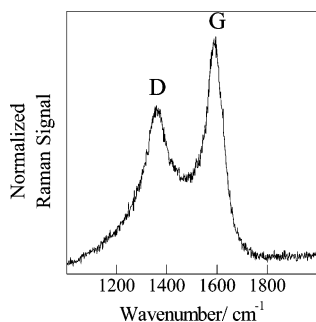


Figure 3. Representative first-order Raman spectrum of a CNF electrode indicating the presence of graphitic defects associated with edge plane graphite.

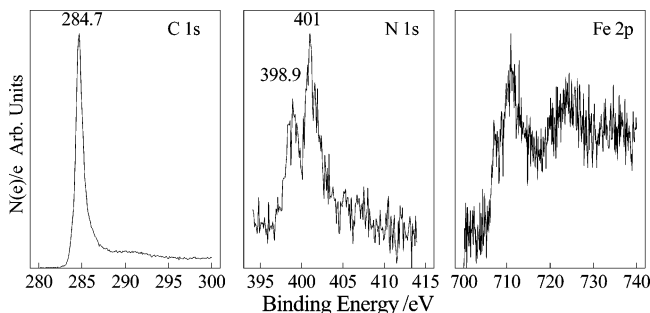


Figure 4. X-ray photoelectron spectra for CNF electrodes. Single-scan spectra for C1s and N1s and a ten-scan averaged spectrum for Fe2p core levels are shown.

defects is shown in Figure 3. The first-order spectra contained two strong peaks near 1360 cm^{-1} and 1590 cm^{-1} , commonly referred to as the D and G bands, respectively. The ratio of D and G band intensities is known to correlate with the in-plane crystal domain size and has been used to estimate the degree of disorder in the graphitic carbon or, conversely, the extent of edge plane graphite.⁴¹ A I_D/I_G ratio near zero indicates high crystallinity (order) and a ratio near to or greater than one demonstrates high disorder due to abundant defects in the graphitic structure. For five different CNF electrodes, we estimated a relative I_D/I_G ratio of 0.75 ± 0.09 (1σ), suggesting that the CNFs are highly disordered and that significant edge plane sites are present. Using the empirical relationship, $L_a = (4.4\text{ nm})(I_G/I_D)$,⁴² we estimate that the average in plane crystalline domain size of our CNFs measured parallel to the basal plane (L_a) is ca. 6 nm. Peak widths of the D and G bands have also been used as an indicator of disorder in graphitic materials.⁴³ As noted by Cuesta et al. for highly disordered graphitic materials, the full width at half-maximum (FWHM) for both bands is observed to increase, along with the I_D/I_G ratio. We also have noticed that our disordered CNF electrodes exhibit broadened FWHMs and show shoulders on the lower energy side of both D and G bands in comparison to more crystalline CNFs grown using non-nitrogen containing precursors. Broadening of the Raman peaks is also reflective of the small crystallite size and has the same characteristic features of microcrystalline carbons.¹ Analysis of the low-frequency Raman spectral range from 200 to 600 cm^{-1} yields no evidence for the presence of iron oxide (Fe_2O_3) on the CNF surface which could result from air oxidation of Fe nanoparticles formed during pyrolysis process.⁴⁴

XPS analyses of the CNF electrodes, Figure 4, indicate that the carbon is predominantly sp^2 hybridized denoted by a C1s binding energy of 284.7 eV, similar to that of HOPG.^{1,45} No detectable sidebands in the C1s region (285–291 eV) are present to suggest the existence of graphene oxides or oxygen-containing

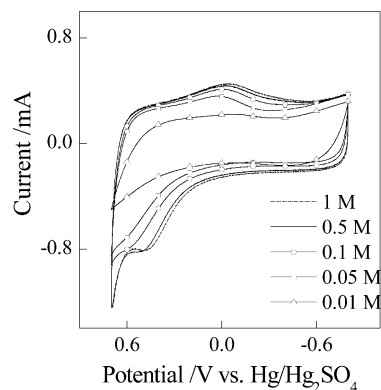


Figure 5. Voltammetric responses of a CNF electrode immersed in deaerated solutions containing various concentrations of KNO_3 . Scan rate: 100 mV/s.

functionalities on the CNF electrodes.¹ A small O1s signal at 532.6 eV (data not shown) is also apparent and implies the presence of adsorbed molecular oxygen or H_2O .⁴⁶ Additionally, the occurrence of a N1s doublet at ~ 398.9 and 401.0 eV is indicative of the incorporation of nitrogen within the graphene sheets.^{47,48} In agreement with similar reports for nitrogen-incorporated carbonaceous materials,^{13,47–49} the binding energy centered at 398.9 eV corresponds to “pyridinic” nitrogen while that at 401.0 eV is commensurate with “pyrrolic”-type nitrogen. The former refers to N atoms that contribute to the π system with one p electron, while the latter refers to N atoms with two p electrons on the π system, although not necessarily coordinated in a pentagonal arrangement as pyrrole.⁴⁷ A very weak peak at ~ 405 eV also exists that is consistent with presence of “graphitic” quaternary nitrogen, corresponding to highly coordinated N atoms substituting inner carbon atoms within the graphene sheets.⁴⁷ A very weak pair of doublets for the $\text{Fe}2\text{p}_{3/2}$ and $\text{Fe}2\text{p}_{1/2}$ signals at 707 and 720 eV and at 711 and 725 eV are seen, suggestive of the presence of metallic iron (or its carbide) and oxidized iron species.^{46,50} Integration of the relative N and Fe elemental abundances indicates that CNFs contain $\sim 1\%$ at. N and $\sim 0.1\%$ at. Fe at the surface.⁵¹ Complementary thermogravimetric analysis (TGA) of these CNFs reveals that the bulk material contains $9 \pm 3\%$ Fe by mass. The supporting Raman, XPS, TEM data back the contention that the majority of iron is entrapped within the interior the CNF structure.

Electrochemical Characterization. CNFs grown by CVD and pyrolysis are known to be strongly hydrophobic as prepared.⁵² Typically, in order for nanotubular carbon materials to be used in electrochemical applications involving aqueous electrolytes, the electrode needs to be preconditioned or pre-treated so that it is easily wetted when immersed in solution. Harsh chemical or electrochemical oxidation methods that use concentrated nitric and sulfuric acids are typically employed to introduce effectively oxygen-containing surface functionalities (carboxyl and carboxylic anhydride groups).⁵³ However, this severe treatment usually leads to breakdown or fracture of the CNF nanostructure.⁵⁴ Our “as prepared” CNF electrodes also do not easily wet, but we have found that very mild electrochemical conditioning by cycling from -1.4 to $+0.8$ V vs $\text{Hg}/\text{Hg}_2\text{SO}_4$ at 100 mV/s in aqueous 1 M KNO_3 for a period of about two minutes induces uniform wetting of the CNF electrodes. This is evidenced by a large increase in the voltammetric current during cycling when the entire CNF electrode fully saturates with electrolyte. Figure 5 shows a typical voltammetric response for wetted CNF electrodes immersed in deaerated solutions containing KNO_3 for potential cycles between $+0.7$ V and -0.8 V vs $\text{Hg}/\text{Hg}_2\text{SO}_4$. Over most

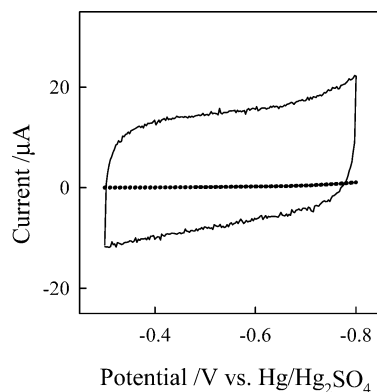


Figure 6. Voltammetric response of a CNF electrode (solid line) and a heat-treated bare nickel mesh electrode (dotted line) immersed in a deaerated solution containing 0.5 M KNO_3 . Scan rate: 1 mV/s.

of the potential range, the voltammogram is nearly featureless with only capacitive charging currents observed. A small peak observed at +0.5 V, near the anodic limit, is indicative of nitrate insertion into the CNFs and is broadly consistent with previous reports for voltammetric investigations of HOPG electrodes in similar electrolytes.⁵⁵ A broad cathodic wave is also seen in this potential range corresponding to the deintercalation of nitrate ions, indicating that the insertion process is reversible. We note that the CNF electrodes are very stable during extended cycling between +0.8 and -0.8 V, and no changes in the voltammetric response is seen to denote the creation of quinone-like or other oxygen-containing functionalities.^{1,5} Typically, anion intercalation is always accompanied by formation of graphene oxide;^{55,56} however, even after extended potential cycling (>100 cycles) we observe no new voltammetric peaks to signify its formation. This mild conditioning step should not be confused with more rigorous electrochemical pretreatment activation (ECP) methods reported by others.^{5,57} We note that the conditions used here are much milder since the CNF electrodes are cycled to much less extreme oxidation potentials (cf. +0.8 V vs +2.2 V vs $\text{Hg}/\text{Hg}_2\text{SO}_4$) for much shorter time periods.⁵⁵ XPS and SEM analysis of wetted electrodes show no changes in the overall CNF composition or structure. First-order Raman spectra for excessively cycled samples also exhibited no spectral differences. TEM analysis was inconclusive in determining if possible structural changes or defects were introduced after the wetting step. Regardless, from the available evidence there appears to be no substantial amount of oxygen-containing surface functional groups inherent to or introduced into the CNF electrodes during the mild electrochemical conditioning process. Since the XPS data indicate that substantial nitrogen-containing functionalities exist on our CNF electrodes, we surmise that mild electrochemical cycling of the electrodes facilitates protonation of basic nitrogen surface sites such as pyridinic groups to produce positively charged pyridinium functionalities.⁴⁷ As a result, a more polar surface is created that is more easily wetted by aqueous electrolyte. This reasoning is consistent with studies of carbons that exhibit a decrease in the water contact angle with an increase in positive surface charge.⁵⁸

Figure 6 shows a representative voltammetric response of a CNF electrode immersed in a deaerated 0.5 M KNO_3 solution, cycled between -0.3 V and -0.8 V. In an O_2 -free solution, the CV exhibits only a capacitive charging response. Notably, the current measured for a CNF-coated nickel mesh electrode is several orders of magnitude higher than that for the uncoated nickel mesh electrode of the same area, indicating that the observed electrochemical response is inherent to the CNF electrode and not the underlying nickel support. As expected,

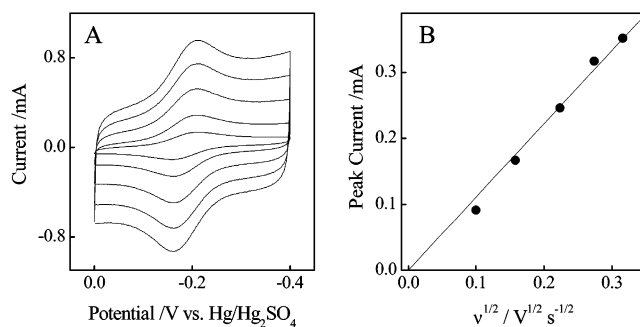


Figure 7. (A) Voltammograms of a CNF electrode immersed in a deaerated solution containing 4 mM $\text{K}_3\text{Fe}(\text{CN})_6$ and 1 M KNO_3 . Scan rates: 10, 25, 50, 75, and 100 mV/s. (B) Plot of cathodic peak currents from (A) versus the square root of the scan rate.

the CNF electrodes exhibit significantly larger background charging currents since the higher surface area leads to a higher overall capacitance. For an electrode scanned at a constant rate, ν , the capacitive current can be expressed as $i = C A \nu$, where A and C correspond to the electrode area and areal capacitance (F cm^{-2}). The gravimetric capacitance of the CNF electrodes can be estimated from voltammograms using $C = (1/2)(i_a - i_c)/\nu$ where i_a and i_c are the anodic and cathodic charging currents observed in Figure 6.⁵⁹ Using this equation to compute C from the voltammetric data at -0.6 V vs $\text{Hg}/\text{Hg}_2\text{SO}_4$, the capacitance was found to be ca. 11 F/g in 1 M KNO_3 . This value is in agreement with the wide range of measured gravimetric capacitance values, ranging been 4 to 80 F/g⁶⁰ and 18 to 40 F/g^{61,62} reported for CNT electrode materials evaluated under similar electrolyte conditions.

The electron-transfer kinetics of the “as prepared” CNF electrodes were also examined using two well-known redox couples. A typical response for the $\text{Fe}(\text{CN})_6^{3-/4-}$ couple is shown in Figure 7. For each redox couple, five different electrodes were studied and scan rates for each electrode were recorded at 25, 50, 75, and 100 mV/s. Peak splittings ($\Delta E_p = E_{pc} - E_{pa}$) for $\text{Ru}(\text{NH}_3)_6^{3+/2+}$ were found to be 57 ± 6 mV, while for $\text{Fe}(\text{CN})_6^{3-/4-}$ were estimated to be 55 ± 2 mV, indicative of fast electron-transfer kinetics with ΔE_p values close to the ideal 59 mV and the i_{pc}/i_{pa} ratio near unity for a reversible one-electron transfer process. In contrast, Li et al.⁶³ measured ΔE_p values ranging from 100 to 168 mV for $\text{Fe}(\text{CN})_6^{3-/4-}$ in 1 M KCl at MWCNT electrodes. Marken et al.⁶⁴ reported similar values of 168 mV for $\text{Ru}(\text{NH}_3)_6^{3+/2+}$ at MWCNT electrodes prepared by comparable routes. Using microelectrode fashioned from a small bundle of MWCNTs, Ajayan et al.⁶⁵ found ~ 59 mV peak splittings for $\text{Fe}(\text{CN})_6^{3-/4-}$ in an unspecified electrolyte. The lack of specific detailed information on the electrode properties prevents direct comparison of electrochemical behaviors between systems. However, we disagree with the authors’ claims⁶⁵ that near-perfect atomically smooth basal plane MWCNT structures promote fast electron transfer kinetics, since it contradicts the abundant evidence⁵ that disorder in the graphite structure increases electronic transfer rates. The fast electron transfer kinetics of our CNF electrodes, inferred by the nearly ideal Nernstian response, suggest that the electron-conducting properties are enhanced beyond that of more perfectly ordered forms carbon (HOPG).⁶⁶ Most likely, our CNF electrodes demonstrate improved electron-transfer kinetics due to reduced “iR” drop as a result of improved electrical contact and, presumably, to edge plane defects induced by incorporation of nitrogen atoms, since these materials are known to possess increased electronic conductivity.⁶⁷ Theoretical calculations by Thrower et al. on N-doping in graphitic carbons support the

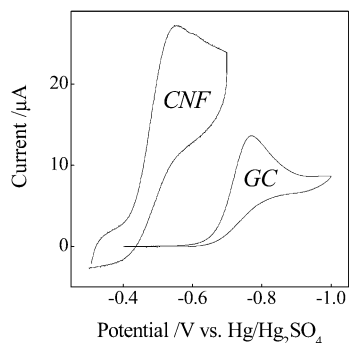


Figure 8. Voltammograms of CNF and glassy carbon (GC) electrodes immersed in a 1 mM O₂-saturated solution containing 1 M KNO₃. Scan rate 5 mV/s.

idea that electron-transfer kinetics and catalytic activities can be accelerated by nitrogen incorporation as a consequence of band gap lowering and increased electron (charge) mobility.⁶⁸ This is backed by strong experimental evidence provided by McCreery et al.,⁶⁹ on well-characterized HOPG electrodes where increased disorder significantly enhances electron transfer rates due to modification of the electronic structure to reduce the band gap and increase the local density of states (LDOS). We also note that the electron transfer kinetics may be significantly altered by surface-exposed functional groups (i.e., nitrogen functionalities) which can promote specific surface interactions and accelerate reaction rates. In particular, the Fe(CN)₆³⁻⁴⁻ redox couple is known to be strongly influenced by electronic factors and reactive surface sites.^{5,69} The observed high capacitance associated with nitrogen functionalities and edge plane sites and the nearly ideal Nernstian response for our CNF electrodes support the idea of the importance of disorder-induced and N-doped electronic effects on redox reactions. Future studies are planned to evaluate more fully the role of electronic properties and reactive sites on CNF electrode kinetics. Nonetheless, the observed facile electron transfer kinetics strongly suggested to us that these N-doped CNFs should also demonstrate enhanced electrochemical behavior for more technologically relevant redox-active analytes (e.g., dioxygen, peroxide).

Electrocatalysis of Dioxygen. To explore the premise that CNFs containing nitrogen were active electrocatalysts, we chose to evaluate the performance of our CNF electrodes toward O₂ reduction using potential step and cyclic voltammetric methods, two techniques used extensively to study O₂ reduction.^{70,71} Moreover, oxygen reduction studies are intriguing since the CNF electrodes are broadly related to heat-treated FePc-modified carbon black electrodes.^{72,73} Historically, metalloporphyrins and metallophthalocyanines have drawn considerable interest as catalytic modifiers for carbon-based electrodes (e.g., carbon blacks and glassy carbon) because they are known to lower the kinetic overpotential for oxygen reduction.⁷⁴ The voltammetry of a CNF electrode immersed in a saturated O₂ solution containing 1 M KNO₃ (pH = 7) is shown in Figure 8, along with the response obtained at a conventionally polished GC electrode. For both electrode materials, a single, cathodic peak is observed, consistent with that for the irreversible reduction of O₂. The peak potential observed at -0.5 V vs Hg/Hg₂SO₄ for the CNF electrode is shifted significantly positive (ca. 300 mV) relative to the response for a GC-based electrode. This positive potential shift implies that the CNF electrodes are more catalytically active (kinetically more facile) for O₂ reduction. Figure 9 shows background-corrected voltammograms for a CNF electrode cycled at different scan rates in a 1 mM O₂ saturated solution containing 1 M KNO₃. The observed peak

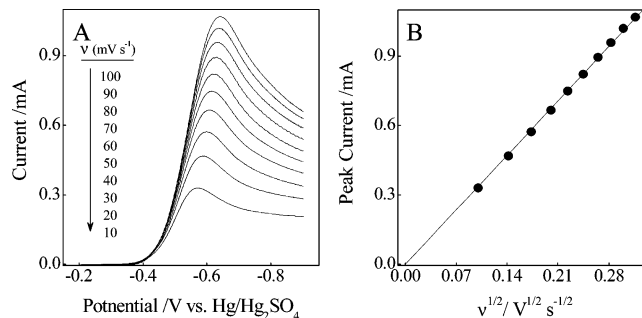


Figure 9. (A) Voltammograms of a CNF electrode immersed in a 1 mM O₂-saturated solution containing 1 M KNO₃ as a function of scan rate. (B) Plot of cathodic peak currents from (A) versus the square root of the scan rate.

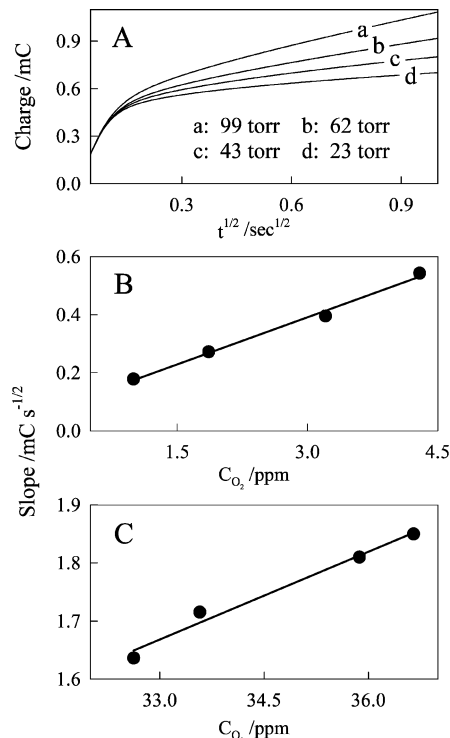


Figure 10. Chronocoulometric responses of a CNF electrode immersed in a solution containing 1 M KNO₃ and indicated amounts of O₂. (A) Plot of charge vs $t^{1/2}$ (Anson plot) measured for solutions under various partial pressures of O₂. (B) and (C) Plots of slopes determined from Anson plots vs dissolved O₂ concentration obtained over two different concentration ranges.

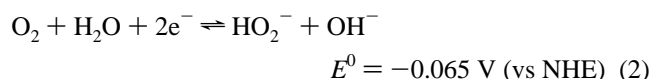
current for O₂ reduction is proportional with the square root of the scan rate (Figure 9B), consistent with a diffusion-controlled process. Using the Randles-Sevcik equation,⁷⁵ we estimate from the slope of this plot a value of $n = 2.0 \pm 0.2$, in accord with the reduction of O₂ to HO₂⁻ by a two-electron process.

A more quantitative assessment of the sensitivity of the CNF electrodes toward dissolved O₂ concentration was performed using chronocoulometry since the effects from the capacitive and faradaic processes can be readily discerned without requiring separate “blank” measurements or background subtraction procedures. Figure 10 shows the influence of O₂ concentration on the chronocoulometry response. As predicted by the integrated Cottrell equation, eq 1, a plot of the total charge passed, Q vs $t^{1/2}$ (Anson plot), should be linear and purely a result of the faradaic process.^{76,77}

$$Q = 2nFAC_0D_0^{1/2}\pi^{-1/2}t^{1/2} \quad (1)$$

Additionally, the slope of the linear portion of this plot is independent of the electrode's capacitance and is directly proportional to the concentration of dissolved oxygen. Figures 10B and 10C show that the change in Anson plot slopes is linear over the studied concentration ranges (1–40 ppm), demonstrating that these CNF electrodes can function quantitatively as O₂ sensors. The number of electrons can also be established from an Anson plot. In agreement with the cyclic voltammetry studies above, we observed an average value of $n = 2.3 \pm 0.3$ for five CNF electrodes examined. If the potential is stepped to a more negative potential, -1.3 V vs Hg/Hg₂SO₄, we observe a 2-fold increase in the Anson plot slope, yielding an average value of $n = 4.0 \pm 0.3$, corresponding to a complete reduction of oxygen and hydrogen peroxide to OH⁻.

The electrocatalytic response of our electrodes is consistent with the well-described behavior for O₂ reduction at carbonaceous electrodes in neutral to alkaline electrolytes. Under such conditions, O₂ reduction primarily proceeds by the peroxide pathway, with the first electron transfer step involving generation of hydroperoxide ion, eq 2.^{78,79}



This reaction may be followed either by a second two-electron reduction of HO₂⁻ to OH⁻, eq 3,



or by the rapid chemical decomposition of HO₂⁻ to regenerate O₂, eq 4.



Although the thermodynamics predict that the reduction of HO₂⁻, should occur at much more positive values than O₂ reduction, a large overpotential is generally required due to slow reduction kinetics. This in effect pushes the HO₂⁻ reduction process more negative of the O₂ reduction potential.⁸⁰ Thus, for most carbon-based electrodes such as GC, generated HO₂⁻ accumulates in solution, since the kinetics are slow for both the second reduction (eq 3) and the chemical decomposition (eq 4) steps.^{81,82}

The kinetics for O₂ reduction can be influenced by many factors (i.e., surface area, amount of edge plane graphite, oxygen functionalities). More insight into the enhanced electrocatalytic activity of our CNF electrodes can be gained by investigating the mechanistic steps for O₂ reduction. From decades of studies, it has been well established that the surface structure has a major influence on O₂ reduction kinetics.^{1,5,83} In particular, surface functionalities at edge plane defects are known to significantly increase O₂ reduction activity by acting as adsorption sites for dioxygen and other intermediates.⁸⁰ McCreery and co-workers⁸⁴ have recently proposed that at metal-free carbon surfaces, O₂ reduction involves surface adsorption of superoxide, with the first step consisting of dioxygen being reduced to superoxide (eq 5), followed by protonation to form hydroperoxide (eq 6) and subsequent reduction (eq 7).

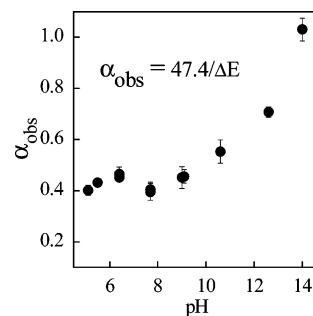
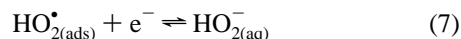
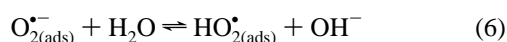
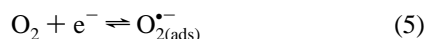


Figure 11. Plot of the apparent charge-transfer coefficient, α_{obs} , vs pH for CNF electrodes immersed in O₂-saturated solutions buffered at specified pHs. Individual data points represent a pooled set of five electrodes measured 10 times each as a function of pH.

In a follow-up study, McCreery and colleagues⁸⁵ discussed their interpretation of voltammetric data to decipher between an adsorptive reduction pathway and a purely outer-sphere reduction pathway. A pH dependence of the observed O₂ reduction potential and on the apparent transfer coefficient, α_{obs} , is a key indicator in distinguishing if the adsorption pathway is predominant. They argued that in neutral to basic pH solutions, a purely outer-sphere mechanism should show a constant $\alpha_{\text{obs}} = 0.5$ and be independent of pH. In contrast, the adsorptive pathway (eq 5) should demonstrate a value of $\alpha_{\text{obs}} = 0.5$ at neutral pH, but increase to a value near $\alpha_{\text{obs}} = 1$ in very basic conditions, reflective of a change in rate-determining steps between eqs 5 and 6. Accordingly, we also collected cyclic voltammograms as a function of pH (data not shown). Figure 11 shows a plot of α_{app} vs pH obtained from a pooled set of five CNF electrodes measured 10 times each at specified pH values in a 1 mM saturated O₂ solution. The value α_{obs} was estimated from the voltammograms using eq 8 for an irreversible reduction process⁸⁶

$$E_{p/2} - E_p = \frac{1.857RT}{\alpha_{\text{obs}}F} \quad (8)$$

where E_p is the potential where the peak current was observed, and $E_{p/2}$ is the potential where the current is exactly one-half the total peak current. Figure 11 shows that at pH < 10 the apparent charge transfer coefficient is nearly independent of pH, exhibiting a constant value near 0.5. However, at pH > 10, α_{app} increases toward 1 with increased alkalinity. The observed pH behavior is consistent with O₂ reduction occurring via an adsorptive reduction pathway where the rate-limiting step is controlled via eq 5 at pH < 10 and by eq 6 at pH > 10. As discussed above, the CNF electrodes prepared herein are structurally disordered and possess dislocations that present exposed N-doped edge plane graphite that possibly serve as adsorption sites. Therefore it is highly likely that CNFs with a large density of kinks and nitrogen functional groups per unit length will exhibit enhanced activity for O₂ reduction, especially in neutral to alkaline solutions. This behavior is in agreement with other studies of disordered carbons with high edge plane site concentrations that demonstrate accelerated O₂ reduction rates.^{1,5,78} This phenomenological model, however, based solely on adsorption at edge planes, does not establish what chemical groups are present and what role they play in affecting O₂ reduction kinetics.

Despite decades of intense research efforts on carbon-supported, heat-treated iron macrocycles, the mechanistic steps associated with O₂ reduction are still poorly understood. Many conflicting studies have been reported and there is still no consensus about the nature of the species formed during

pyrolysis and which of them enhance O₂ electrocatalysis. The majority of evidence indicates that the most active and stable catalysts are achieved when precursors containing carbon, iron, and nitrogen are pyrolyzed at 700–1000 °C.^{72,73,87–89} Dodelet and others have long speculated that decomposition of N₄–Fe macrocycles create FeN₂/C- and FeN₄/C-type catalytic sites on carbon with Fe coordinated in 1,10-phenanthroline-like arrangements within graphene planes.⁹⁰ However, many do not support this view because the high activity observed does not necessarily require the presence of Fe, and that catalytically active materials can be prepared on virtually any carbon support using a variety of Fe- and N-containing precursors, including even those made by pyrolyzing iron(II) acetate on carbon in NH₃.^{78,91} In our case, it is highly unlikely that intact or decomposed FePc is present since the CNF growth temperature employed (~1000 °C) is well above the temperature (<600 °C) where most transition metal macrocycles are known to be thermally stable.⁹² Additionally, voltammograms for CNF electrodes in deaerated solutions (Figures 5 and 6) showed neither of the described, reversible peaks for Fe(II)/Fe(III) or the Fe(0)/Fe(II) redox couples of FePc.^{72,74,93} We also do not think that metallic Fe or Fe-containing pyrolysis products are catalytically active for O₂ reduction since the data presented herein backs the observations by others^{38,39,72} that the majority of Fe is encapsulated within graphitic envelopes or within the CNF interior. This premise is further supported by the fact that we observe no voltammetric peaks such as those reported by Savinell et al.⁹⁴ indicative for the anodic stripping/dissolution of metallic iron, iron hydroxides or oxides from the carbon surface. Therefore, it appears highly unlikely that O₂ reduction at our CNF electrodes proceeds via Fe-redox mediation-type mechanism, typical for most intact iron macrocycles supported on carbon electrodes.^{74,95} We note that electrocatalysis of O₂ in more acidic solutions (pH < 2) is likely to be more complicated since Fe readily dissolves in concentrated acids and Fe ions can rebind to act as redox-active catalytic sites.^{72,78}

In our opinion, the most plausible mechanism for increased catalytic activity supports the original conjecture of Yeager⁷⁸ that nitrogen functionalities are associated with the active center for oxygen reduction. As detailed above, there is considerable nitrogen content (~1 at. %) in our CNF electrodes coordinated in possibly two or three different ways. We believe that the increased catalytic activity and more the positive O₂ reduction potential observed for our CNF electrodes is predominantly a result of enhanced adsorption at nitrogen functional groups which proceeds to accelerate O₂ reduction and advance heterogeneous peroxide decomposition. We speculate that Fe predominantly acts to promote and stabilize nitrogen incorporation into the graphene sheets by serving as a catalytic growth agent during the CNF formation. Recent investigations³⁸ on CNT growth from FePc precursors support the idea that decomposing phthalocyanine molecules dissolve into molten catalytic Fe particles and dissolved N atoms precipitate with the carbons, resulting in N-doping of the CNTs. This is in accord with the early work of Mrha⁹⁶ and recent studies of Biniack et al.⁹⁷ on NH₃ activation of graphitic carbons and consistent with the original hypothesis from Yeager's group,^{78,98} that the presence of Fe during pyrolysis stabilizes the binding of nitrogen to the surface. Recent experiments conducted in our laboratory on N-doped and undoped CNFs reveal the importance of nitrogen functionalities.⁹⁹ High O₂ electrocatalytic activity and fast peroxide decomposition is observed only with nitrogen-containing CNFs even when N-doped and undoped CNFs possess the same structural characteristics and Fe loadings. In the absence

of nitrogen doping, the O₂ reduction potential is shifted significantly more negative and the second electrochemical reduction of hydroperoxide to hydroxide (eq 3) is evident. Recent simulations in our group of linear sweep voltammetry based on the mechanism put forth by McCreery^{84,85} strongly suggest that the observed positive shift in O₂ reduction potential at N-doped CNF electrodes is a direct result of activated surface adsorption of superoxide (eq 5) at basic surface functionalities. These sites also accelerate proton transfer to form hydroperoxide which then rapidly disproportionates to regenerate oxygen (eq 7).⁹⁹ This hypothesis is supported by the recent results of Biniack et al.⁹⁷ on porous carbons that found a strong correlation between the O₂ reduction potential and incorporated nitrogen content on the heterogeneous rate constant for hydrogen peroxide decomposition. Future studies are planned to elucidate the chemical and structural nature of the nitrogen active site in our CNF electrodes.

Summary

The CNF electrodes conveniently prepared on conductive substrates by pyrolysis of FePc in a reducing atmosphere possess interesting properties for preparation of electrocatalytic electrodes and electrochemical O₂ sensors. A key feature of this preparation methodology is that the growth conditions can be precisely adjusted³⁸ to control CNF structure, orientation, and composition in an effort to optimize electrochemical performance. Preliminary studies of "as-grown" N-doped CNF electrodes suggest that incorporation of nitrogen improves the inherent electrical and electron-transfer properties, in addition to promoting adsorption and enhancing the electrocatalytic activity for O₂ reduction. A tentative mechanism is proposed similar to that of McCreery⁸⁵ where in pH < 10 solutions, the reduction of O₂ proceeds by a two-electron process with the rate-limiting step controlled by adsorbed superoxide at surface nitrogen groups. In pH > 10 solutions, the adsorption process is reduced, presumably due to deprotonation of basic nitrogen functionalities, and is limited by rate of protonation of superoxide. The ability to prepare CNFs directly on conductive supports with tuned chemical and structural properties may prove useful for implementation in advanced sensors, batteries, and fuel cells.

Acknowledgment. Financial support of this work was provided in part by the Welch Foundation (Grant F-1529) and NSF. S.M. acknowledges the Harrington Foundation and the NSF for fellowship support.

References and Notes

- (1) Kinoshita, K. *Carbon: Electrochemical and Physicochemical Properties*; John Wiley: New York, 1988.
- (2) Baker, R. T. K. *Carbon* **1989**, 27 (3), 315.
- (3) Rodriguez, N. M. *J. Mater. Res.* **1993**, 8 (12), 3233.
- (4) Sinnott, S. B.; Andrews, R. *Crit. Rev. Solid State Mater. Sci.* **2001**, 26, 145.
- (5) McCreery, R. L. In *Electroanalytical Chemistry*; Bard, A. J., Ed.; Marcel Dekker: New York, 1991; Vol. 17.
- (6) De Jong, K. P.; Geus, J. W. *Catal. Rev. Sci. Eng.* **2000**, 42 (4), 481.
- (7) Rao, A. M.; Richter, E.; Bandow, S.; Chase, B.; Eklund, P. C.; Williams, K. A.; Fang, S.; Subbaswamy, K. R.; Menon, M.; Thess, A.; Smalley, R. E.; Dresselhaus, G.; Dresselhaus, M. S. *Science* **1997**, 275 (5297), 187.
- (8) Besenhard, J. O.; Fritz, H. P. *Angew. Chem., Int. Ed. Engl.* **1983**, 22, 950.
- (9) De Heer, W. A.; Chatelain, A.; Ugarte, D. *Science* **1995**, 270 (5239), 1179.
- (10) Endo, M.; Kim, Y. A.; Matusita, T.; Hayashi, T. *Proceedings of the NATO Advanced Study Institute on Carbon Filaments and Nanotubes*:

- Common Origins, Differing Applications*; Biro, L. P., Bernard, C. A., Tibbetts, G. G., Lambin, P., Eds.; Kluwer Academic Publishers: The Netherlands, 2001; pp 51–61.
- (11) Endo, M.; Takeuchi, K.; Igarashi, S.; Kobori, K.; Shiraishi, M.; Kroto, H. W. *Phys. Chem. Solids* **1993**, *54*, 1841.
- (12) Masuda, T.; Mukai, S. R.; Hashimoto, K. *Carbon* **1993**, *31* (5), 783.
- (13) Yudasaka, M.; Kikuchi, R.; Ohki, Y.; Yoshimura, S. *Carbon* **1997**, *35* (2), 195.
- (14) Huang, S.; Dai, L.; Mau, A. W. H. *J. Phys. Chem. B* **1999**, *103* (21), 4223.
- (15) For a recent review, see: Rao, C. N. R.; Govindaraj, A. *Acc. Chem. Res.* **2002**, *35*, 998.
- (16) Smiljanic, O.; Dellero, T.; Serventi, A.; Lebrun, G.; Stansfield, B. L.; Dodelet, J. P.; Trudeau, M.; Désilets, S. *Chem. Phys. Lett.* **2001**, *342* (5), 503.
- (17) Vander Wal, R. L.; Hall, L. J.; Berger, G. M. *J. Phys. Chem. B* **2003**, *106* (51), 13122.
- (18) Zhao, J.; Gao, Q. Y.; Gu, C.; Yang, Y. *Chem. Phys. Lett.* **2002**, *358* (1), 2002.
- (19) Chem, J. H.; Li, W. Z.; Wang, D. Z.; Yang, S. X.; Wen, J. G.; Ren, Z. F. *Carbon* **2002**, *40* (8), 1193.
- (20) Li, J.; Cassell, A.; Delzeit, L.; Han, J.; Meyyappan, M. *J. Phys. Chem. B* **2002**, *106* (36), 9299.
- (21) Luo, Y.; Vander Wal, R.; Hall, L. J.; Scherson, D. A. *Electrochem. Solid-State Lett.* **2003**, *6* (3), A56.
- (22) Davis, J. J.; Coles, R. J.; Hill, H. A. O. *J. Electroanal. Chem.* **1997**, *440* (2), 279.
- (23) Liu, C.; Bard, A. J.; Wudl, F.; Weitz, I.; Heath, J. R. *Electrochem. Solid-State Lett.* **1999**, *2* (11), 577.
- (24) Barisci, J. N.; Wallace, G. G.; Baughman, R. H. *Electrochim. Acta* **2000**, *46* (4), 509.
- (25) Shui, X.; Frysz, C. A.; Chung, D. D. L. *Carbon* **1997**, *35* (10), 1439.
- (26) Liu, P. F.; Hu, J. H. *Sens. Actuators B* **2002**, *84* (2–3), 194.
- (27) Niu, C.; Sichel, E. K.; Hoch, R.; Moy, D.; Tennent, H. *Appl. Phys. Lett.* **1997**, *70* (11), 1480.
- (28) Ye, J. S.; Wen, Y.; Zhang, W. D.; Gan, L. M.; Xu, G. Q.; Sheu, F. S. *Electrochem. Commun.* **2004**, *6* (1), 66.
- (29) Hughes, M. *Adv. Mater.* **2002**, *14* (5), 382.
- (30) Yang, Z.; Wu, H. *Chem. Phys. Lett.* **2001**, *343* (3), 235.
- (31) An, K. H.; Kim, W. S.; Park, Y. S.; Moon, J.; Bae, D. J.; Lim, S. C.; Lee, Y. S.; Lee, Y. H. *Adv. Funct. Mater.* **2001**, *11* (5), 387.
- (32) Wang, Q.; Chen, L.; Huang, X. *Electrochem. Solid-State Lett.* **2002**, *5* (9), A188.
- (33) Shin, H.; Liu, M.; Sadanadan, B.; Rao, A. M. *J. Power Sources* **2002**, *112* (1), 216.
- (34) Britto, P. J.; Santhanam, K. S. V.; Rubio, A.; Alonso, J. A.; Ajayan, P. M. *Adv. Mater.* **1999**, *11* (2), 154.
- (35) Yang, Z.; Wu, H.; Simard, B. *Electrochem. Commun.* **2002**, *4* (7), 574.
- (36) MacArthur, C. G. *J. Phys. Chem.* **1916**, *20* (6), 495.
- (37) Gubbins, K. E.; Walker, R. D. *J. Electrochem. Soc.* **1965**, *112*, 469.
- (38) Kim, N. S.; Lee, Y. T.; Park, J.; Han, J. B.; Choi, Y. S.; Choi, S. Y.; Choo, J.; Lee, G. H. *J. Phys. Chem. B* **2003**, *107* (35), 9249.
- (39) Wang, X.; Hu, W.; Liu, Y.; Long, C.; Xu, Y.; Zhou, S.; Zhu, D.; Dai, L. *Carbon* **2001**, *39* (10), 1533.
- (40) Tuinstra, F.; Koenig, J. L. *J. Chem. Phys.* **1970**, *53* (3), 1126.
- (41) Tuinstra, F.; Koenig, J. L. *J. Comput. Mater.* **1970**, *4*, 492.
- (42) Knight, D. S.; White, W. B. *J. Mater. Res.* **1989**, *4* (2), 385.
- (43) Cuesta, A.; Dhamelincourt, P.; Laureyns, J.; Martínez-Alonso, A.; Tascon, J. M. D. *Carbon* **1994**, *32* (8), 1523.
- (44) Hou, H.; Jun, Z.; Weller, F.; Greiner, A. *Chem. Mater.* **2003**, *15* (16), 3170.
- (45) Poirier, D. M.; Weaver, J. H. *Surf. Sci. Spectra* **1994**, *2* (3), 232.
- (46) Choudhury, T.; Saied, S. O.; Sullivan, J. L.; Abbot, A. M. *J. Phys. D: Appl. Phys.* **1989**, *22* (11), 1185.
- (47) Pels, J. R.; Kapteijn, F.; Moulijn, J. A.; Zhu, Q.; Thomas, K. M. *Carbon* **1995**, *33* (11), 1641.
- (48) Casnovas, J.; Ricart, J. M.; Rubio, J.; Illas, F.; Jiménez-Mateos, J. M. *J. Am. Chem. Soc.* **1996**, *118* (34), 8071.
- (49) Stöhr, B.; Boehm, H. P.; Schlögl, R. *Carbon* **1991**, *29* (6), 707.
- (50) Sethuraman, A. R.; Stencel, J. M.; Rubel, A. M.; Cavin, B.; Hubbard, C. R. *J. Vac. Sci. Technol. A* **1994**, *12* (2), 443.
- (51) XPS sensitivities for elements such as N and Fe are poor. Detection limits on the order of 0.1%–1%. See for example: Nebesny, K. W.; Maschhoff, B. L.; Armstrong, N. A. *Anal. Chem.* **1989**, *61*, 469A.
- (52) Li, H.; Wang, X.; Song, Y.; Liu, Y.; Li, Q.; Jiang, L.; Zhu, D. *Angew. Chem., Int. Ed.* **2001**, *40* (9), 1743.
- (53) Esumi, K.; Ishigami, M.; Nakajima, A.; Sawada, K.; Honda, H. *Carbon* **1996**, *34* (2), 279.
- (54) Ros, T. G.; Van Dillen, A. J.; Geus, J. W.; Koningsberger, D. C. *Chem. Eur. J.* **2002**, *8* (5), 1151.
- (55) Goss, C. A.; Brumfield, J. C.; Goss, C. A.; Irene, E. A.; Murray, R. W. *Anal. Chem.* **1993**, *65* (10), 1378.
- (56) Alsmayer, D. C.; McCreery, R. L. *Anal. Chem.* **1992**, *64* (14), 1528.
- (57) Engstrom, R. C.; Strasser, V. A. *Anal. Chem.* **1984**, *56* (2), 136.
- (58) Conway, B. E. *Electrochemical Supercapacitors: Scientific Fundamentals and Technological Applications*; Kluwer: New York, 1999; pp 189–90.
- (59) Conway, B. E. *Electrochemical Supercapacitors: Scientific Fundamentals and Technological Applications*; Kluwer: New York, 1999; p 57.
- (60) Frackowiak, E.; Mettenier, K.; Bertagna, V.; Beguin, F. *Appl. Phys. Lett.* **2000**, *77* (15), 2421.
- (61) Barisci, J.; Wallace, G.; Baughman, R. *J. Electrochem. Soc.* **2000**, *147* (12), 4580.
- (62) Barisci, J.; Wallace, G.; Chattopadhyay, D.; Papadimitrakopoulos, F.; Baughman, R. *J. Electrochem. Soc.* **2003**, *150* (9), E409.
- (63) Li, J.; Cassell, A.; Delzeit, L.; Han, J.; Meyyappan, M. *J. Phys. Chem. B* **2002**, *106* (1), 9299.
- (64) Murphy, M. A.; Wilcox, G. D.; Dahm, R. H.; Marken, F. *Electrochem. Commun.* **2003**, *5* (1), 51.
- (65) Nugent, J. M.; Santhanam, K. S. V.; Rubio, A.; Ajayan, P. M. *Nano Lett.* **2001**, *1* (2), 87.
- (66) Typically, electron-transfer rate constants can be estimated from cyclic voltammetry data using Nicholson analysis of peak potential and scan rate. For more information see: Nicholson, R. S. *Anal. Chem.* **1965**, *37*, 1351. Due to the high electrode capacitance and the lack of appreciable peak splitting even at fast scan rates we were unable to estimate rate constants via this approach.
- (67) Czerw, R.; Terrones, M.; Charlier, J.-C.; Blasé, X.; Foley, B.; Kamalakaran, R.; Grobert, N.; Terrones, H.; Tekleab, D.; Ajayan, P. M.; Blau, W.; Ruhle, M.; Carroll, D. L. *Nano Lett.* **2001**, *1* (9), 457.
- (68) Strelko, V. V.; Kuts, V. S.; Thrower, P. A. *Carbon* **2000**, *38* (10), 1499.
- (69) Cline, K. K.; McDermott, M. T.; McCreery, R. L. *J. Phys. Chem.* **1994**, *98* (20), 5314.
- (70) McIntyre, J. D. E. *J. Phys. Chem.* **1967**, *71* (5), 1196.
- (71) McIntyre, R.; Scherson, D.; Storck, W.; Gerischer, H. *Electrochim. Acta* **1987**, *32* (1), 51.
- (72) Tanaka, A. A.; Fierro, C.; Scherson, D.; Yeager, E. B. *J. Phys. Chem.* **1987**, *91* (14), 3799.
- (73) Lalonde, G.; Faubert, G.; Côté, R.; Guay, D.; Dodelet, J. P.; Weng, L. T.; Bertrand, P. *J. Power Sources* **1996**, *61* (2), 227.
- (74) Van Der Putten, A.; Elzing, A.; Visscher, W.; Barendrecht, E. *J. Electroanal. Chem.* **1987**, *221* (1), 95.
- (75) Bard, A. J.; Faulkner, L. R. *Electrochemical Methods: Fundamentals and Applications*, 2nd ed.; John Wiley: New York, 2001; p 231.
- (76) Bard, A. J.; Faulkner, L. R. *Electrochemical Methods: Fundamentals and Applications*, 2nd ed.; John Wiley: New York, 2001; p 211.
- (77) Anson, F. *Anal. Chem.* **1966**, *38* (1), 54.
- (78) Yeager, B. *Electrochim. Acta* **1984**, *29* (11), 1527.
- (79) Brito, P. S. D.; Sequira, C. A. C. *J. Power Sources* **1994**, *52* (1), 1.
- (80) Lovrecek, B.; Batinic, M.; Caja, J. *Electrochim. Acta* **1983**, *28* (5), 685.
- (81) Venkatachalapathy, R.; Guadalupe, P. D.; Prakash, J. *Electrochem. Commun.* **1991**, *1* (12), 614.
- (82) Morcos, I.; Yeager, E. *Electrochim. Acta* **1970**, *15* (6), 953.
- (83) Appleby, A. J.; Marie, J. *Electrochim. Acta* **1979**, *24*, 195.
- (84) Xu, J.; Huang, W.; McCreery, R. L. *J. Electroanal. Chem.* **1996**, *410* (2), 235.
- (85) Yang, H. H.; McCreery, R. L. *J. Electroanal. Chem.* **2000**, *147* (9), 3420.
- (86) Bard, A. J.; Faulkner, L. R. *Electrochemical Methods: Fundamentals and Applications*, 2nd ed.; John Wiley: New York, 2001; p 236.
- (87) Lefevre, M.; Dodelet, J. P.; Bertrand, P. *J. Phys. Chem. B* **2002**, *106* (33), 8705.
- (88) Kalvelage, H.; Mecklenburg, A.; Kunz, U.; Hoffmann, U. *Chem. Eng. Technol.* **2000**, *23* (9), 803.
- (89) Lefevre, M.; Dodelet, J. P. *Electrochim. Acta* **2003**, *48*, 2749.
- (90) Lefevre, M.; Dodelet, J. P.; Bertrand, P. *J. Phys. Chem. B* **2000**, *104* (47), 11238.
- (91) Jaouen, F.; Marcotte, S.; Dodelet, J. P.; Lindberg, G. *J. Phys. Chem. B* **2003**, *107* (6), 1376.
- (92) Scherson, D. A.; Fierro, C. A.; Tryk, D.; Gupta, S. L.; Yeager, E. B.; Eldridge, J.; Hoffman, R. W. *J. Electroanal. Chem.* **1985**, *184* (2), 419.
- (93) Wiesner, K. *Electrochim. Acta* **1986**, *31* (8), 1073.
- (94) Gojkovic, S. Lj.; Gupta, S.; Savinell, R. F. *J. Electrochem. Soc.* **1998**, *145*, 3493.
- (95) Shigehara, R.; Anson, F. J. *Phys. Chem.* **1982**, *86*, 2776.
- (96) Mrha, J. *Collect. Czech. Chem. Commun.* **1967**, *32*, 708.
- (97) Biniak, S.; Walczyk, M.; Szymanski, G. S. *Fuel Process. Technol.* **2002**, *79* (3), 251.
- (98) Scherson, D.; Tanaka, A. A.; Gupta, S. L.; Tryk, D.; Fierro, C.; Holze, R.; Yeager, E. B. *Electrochim. Acta* **1986**, *31* (10), 1247.
- (99) Maldonado, S.; Stevenson, K. J. Manuscript in preparation.